The Hybrid Parallel Plates Gas Counter for Medical Imaging

F. Anulli, G. Bencivenni, C. D'Ambrosio, D. Domenici, G. Felici, F. Murtas
Laboratori Nazionali di Frascati - INFN, Via E. Fermi 40, I-00044 Frascati, Italy
C. Morone
Dipartimento di Biopatologia e Diagnostica per immagini, Universit à Tor Vergata, Roma, Italy

We present a study of a multilayer Hybrid Parallel Plates Gas Counter (HPPC) with high spatial and time resolution for the detection of X and gamma photons in medical imaging. The main applications are the diagnostic techniques of SPECT (Single Photon Emission Computed Tomography) and PET (Positron Emission Tomography).
The detector design has been finalized and the performances have been extensively simulated with the FLUKA package. The results show that this kind of detector may represent a valuable alternative to the more expensive scintillator crystals in the medical applications.

1. The SPECT and PET diagnostic techniques

SPECT[1] and PET[2] represent a remarkable exploiting of nuclear physics in the medicine field. The operating principle foresees the injection of a suitable pharmaceutical marked with a radioactive isotope inside the patient. The concentration levels of the pharmaceutical are then measured by the detection of the emitted radiation, providing both morphologic and physiologic informations about the organ under study.

The standard radionuclide for SPECT is the ^{99m}Tc, which emits a photon of energy 141 keV, with a half-life of 6 hr. A very common tracer in PET is the ^{18}FDG (fluorodeoxyglucose), undergoing a β^+ decay with a half-life of 110 min. The annihilation of the outcoming positron produces two almost anti-collinear photons of energy 511 keV, that can be detected in a coincidence.

A typical SPECT or PET scanner is made of one or more rings of detector blocks surrounding the patient. In the SPECT a lead collimator is used in order to limit the impinging angle of the photons, while in the PET lead septa are usually placed between adjacent rings of detectors (*2D acquisition mode*). In the *3D acquisition mode* the septa are removed and coincidences coming from different rings are accepted, thus increasing the detection efficiency and the acceptance angle, but also multiplying the background rate, which can be reduced with appropriate corrections.

All the bi-dimensional projections of the concentration levels, obtained at different angles, are then processed and through a tomographic reconstruction a three-dimensional image is eventually achieved.

Scintillator crystals coupled to position-sensitive photo-multiplier are widely used detectors in nuclear medicine. They provide excellent efficiency, good space and time resolution, but are expensive and have some intrinsic limitations, like a poor determination of the Depth Of Interaction, which will be closely discussed in Sec. 3.

2. Hybrid Parallel Plate Chamber

The Hybrid Parallel Plate Chamber (HPPC) is a gaseous detector following the principle of operation of the Resistive Plate Counters (RPC, Fig. 1 [3]). A

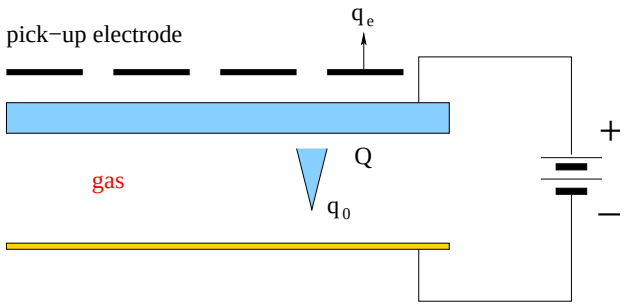

Figure 1: Sketch of the Resistive Plate Chamber.

high, constant and uniform electric field (few kV/mm) is applied between two parallel electrodes. The anode is a 550 μm float glass, operating as resistive electrode, needed to limit the dimension of the avalanche and to avoid a complete discharge. The high voltage is applied and distributed on the external surface of the glass through a resistive coating ($\sim$ 1 M$\Omega/\Box$). The cathode is a thin (3 μm) gold deposition on a kapton substrate (50 μm thick), acting also as the photon converter. The 0.5 mm gas gap defined by the electrodes is flushed with a $C_2H_2F_4 : iC_4H_{10} : SF_6 = 95 : 4 : 1$ gas mixture. The high ionization potential of the low-energy electrons produced by the photoelectric and Compton conversions, allows the detector to be operated in avalanche mode. In fact, despite the sub-millimetric gas gap, the large number of primary clusters available provides an efficiency greater than 80% for charged particles.

The thin gap, together with the fast and dense freon based gas mixture and a suitable readout electronics, allows to achieve a time resolution of $\sim$100 ps. With such a fast detector response a short coincidence window can be used, thus rejecting most of the random

hits, and enhancing the image quality.

The use of a resistive material as an electrode allows the induction of the signal on external readout electrodes, consisting of a double layer of orthogonal copper strips, which provide a bi-dimensional spatial information. The strips are obtained as a 5 μm copper deposition on a 50 μm kapton foil, with the same technique of printed circuit boards. The layer directly faced to the glass electrode has 80 μm wide strips spaced by a 400 μm pitch. The layer behind it has instead 350 μm wide strips, with the same pitch of 400 μm . The different widths permit roughly an equal sharing of the induced charge on the two planes.

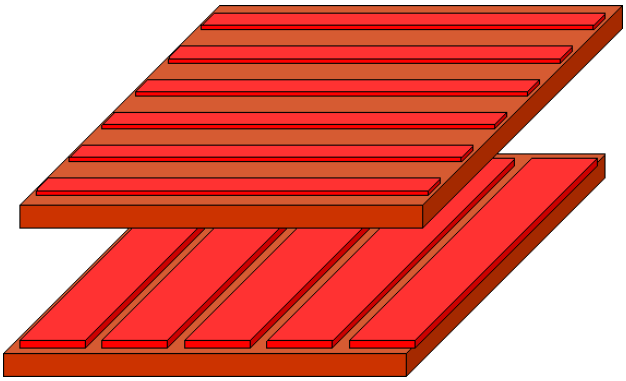

Figure 2: The readout planes of the HPPC are obtained with copper strips deposited on two overlapped kapton foils.

In this very first prototype the strips have been grouped into a 10-fold analog OR, in order to limit the acquisition channels. A 4 mm equivalent pitch is thus obtained, resulting in a 1.15 mm spatial resolution ($\sigma_{res} = pitch/\sqrt{12}$) in both directions. A sub-millimetric spatial resolution can be reached, simply reducing the grouping of the strips and consistently increasing the number of read-out channels, with an intrinsic limit at 115 μm .

In order to achieve a reasonable photon conversion efficiency a multilayer structure is created, by stacking 50 single HPPC elements, as shown in Fig. 3. The signal from each single plane is independently read-out, providing an accuracy as good as 1 mm along the trans-axial direction.

A first prototype consisting of a single gap has been already assembled and tested with cosmic rays, in order to characterize the operating parameters, such as gas gain, read-out setup and front-end electronics. The final 50 gaps detector is under construction and will be tested with radioactive tracers. Its design has been extensively simulated, showing to perform as a suitable detector for medical imaging, and a valuable alternative to the more expensive scintillating crystal detectors.

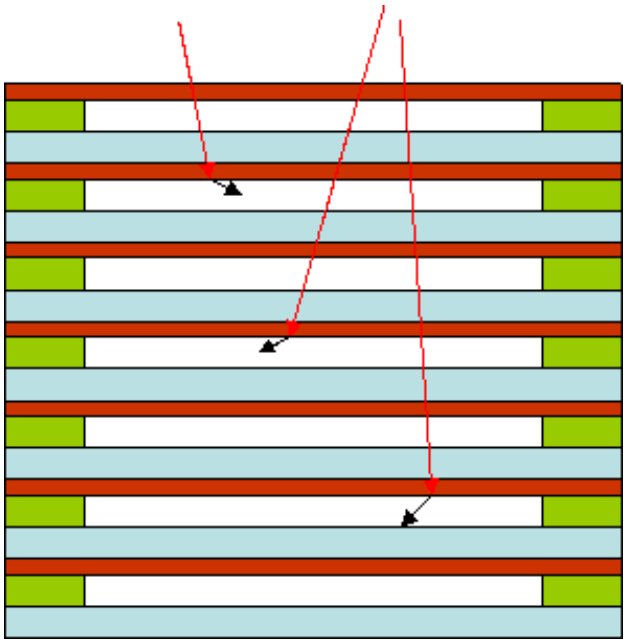

Figure 3: Structure of the HPPC. Several planes are stacked and the signals are independently readout for each plane

3. Imaging capabilities

There are three main sources of degradation of a PET image.

- The random coincidences in opposite detector blocks, coming from uncorrelated events, although simulating a positron annihilation, results in fake reconstruction points and image artifacts. A narrow time window coincidence helps in reducing this background.
- Photons can scatter inside the tissues changing direction and causing a displaced reconstructed decay point. The interaction can be detected by measuring the energy of the photons.
- Photons emitted far from the tomographic axis can happen to interact at a certain depth inside the detector block. As a consequence a parallax error with respect to the actual photons line of flight is produced. A precise determination of the Depth Of Interaction (DOI) in the detector reduces or even eliminate the error.

The HPPC ends up to be rather suitable in the correction of the first and the last classes of events. A time resolution of hundreds of picoseconds allows to use a very short time window, and the combinatorics is thus greatly reduced. Moreover, the high granularity of the detector along the longitudinal direction permits the determination of the DOI with a millimetric resolution, maybe impossible to reach for a scintillating crystal.

Combining this information with the precise measurement of the time of flight of the photons, the coordinate of the annihilation point along the line of flight can be estimated with a precision of few centimeters. Taking into account this constraint during the tomographic reconstruction considerably improves the image quality.

4. Simulation results

The performances of the detector have been extensively simulated with the FLUKA package[4].

4.1. Efficiency

Fig.4 shows that the conversion efficiency for 511 keV photons increases with the thickness of the golden layer on the cathode, while for 140 keV photons a peak value at 3μm is obtained, due to the re-absorption of the low energy electrons inside the conversion material itself.

In order to better understand the various mechanisms contributing to the detector efficiency, two quantities have been defined and studied. The *electron yield* is defined as:

$$EY = \frac{\#e^- \; detected}{\#e^- \; produced} \; ,$$

and the conversion efficiency is defined as:

$$E_\gamma = \frac{\#e^- \; produced}{\#\gamma \; incoming} \; .$$

It is straightforward to prove that the total efficiency is the product of the two:

$$E_{tot} = \frac{\#e^- \; detected}{\#\gamma \; incoming} = EY \times E_\gamma \; .$$

These three quantities are plotted in Fig. 5 as a function of the thickness of the glass electrode and the number of active layers.

As expected, the row conversion efficiency increases with the thickness of the electrode, because more and more photons undergo a Compton scattering in the glass. On the other hand the electron yield decreases, because less and less electrons manage to reach the gas gap leaving a detectable signal. The overall efficiency, being the result of the two opposite mechanisms, is roughly independent from the glass thickness.

On the other hand the electron yield is independent from the number of active layers, because the passive material does not change within a layer, but the conversion efficiency steadily increases. As a result the total efficiency increases with the number of planes.

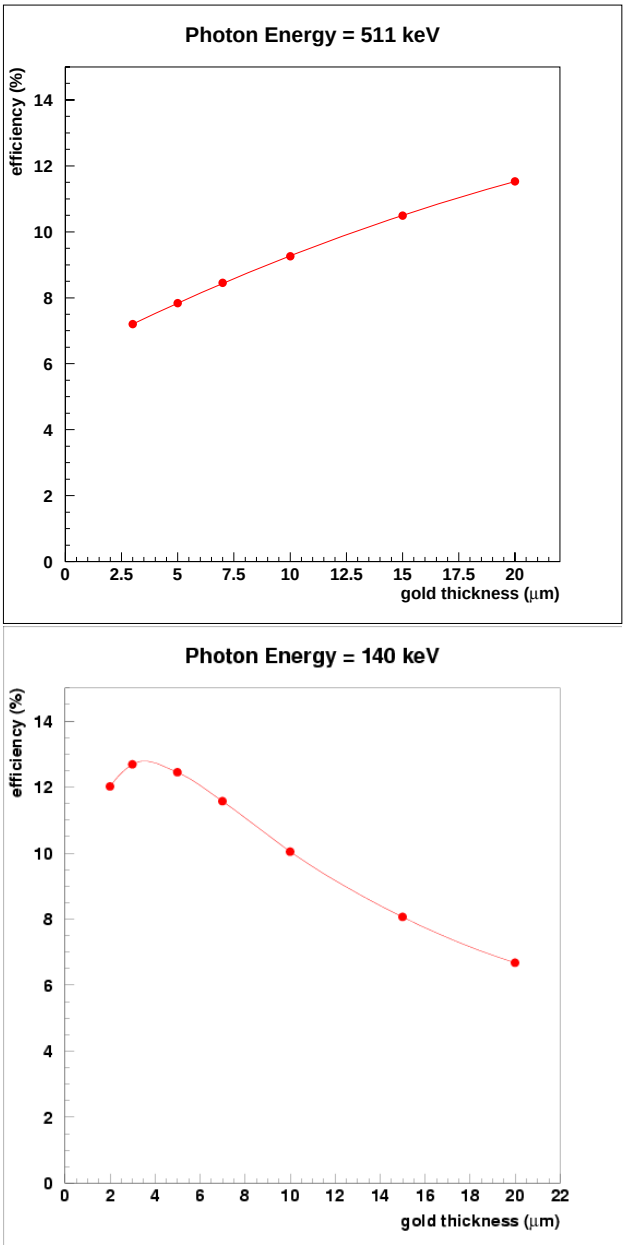

Figure 4: Simulated conversion efficiency for 511 keV PET photons (above), and for 140 keV SPECT photons (below) on the HPPC detector, as a function of the thickness of the cathode golden layer.

These results suggest that a profitable recipe for the detector layout would be to reduce the amount of passive material as much as possible, while stacking as many layers as possible.

4.2. Spatial resolution

The intrinsic resolving power of the detector has been comprehensively studied as well. Fig. 6 shows the points in 3d-space where the photons from two gaussian sources (511 keV energy) interact inside the

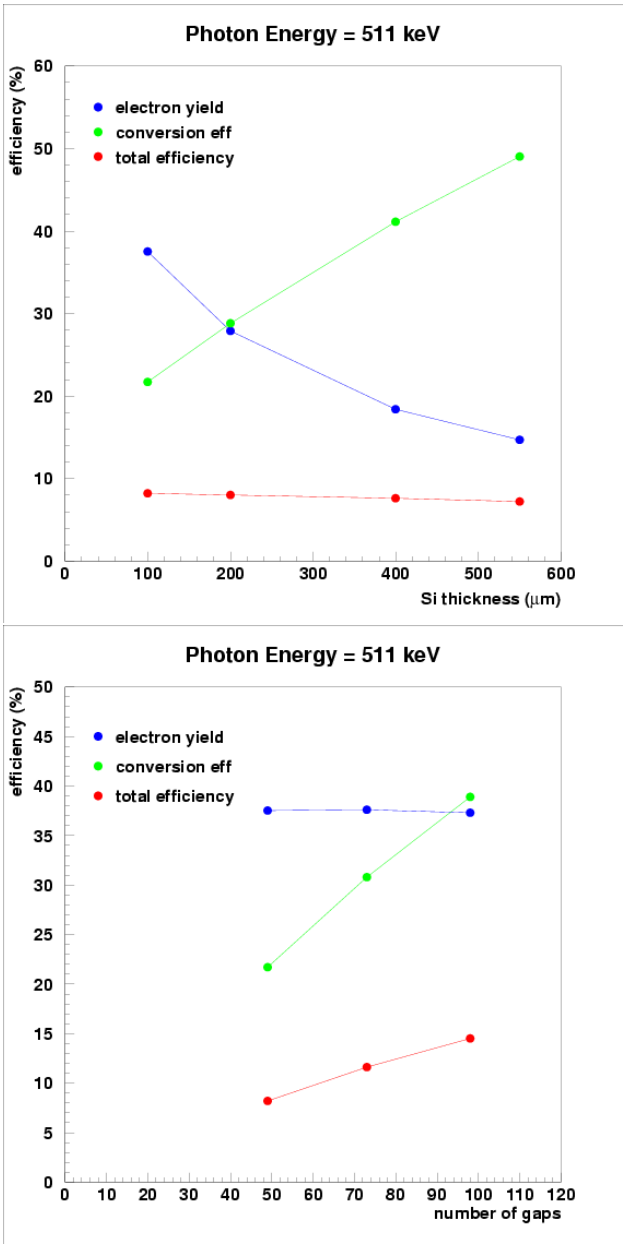

Figure 5: The electron yield, the conversion efficiency and the total efficiency plotted as a function of the thickness of the glass electrode (above), and as a function of the number of HPPC layers (below). The three quantities are defined in the text.

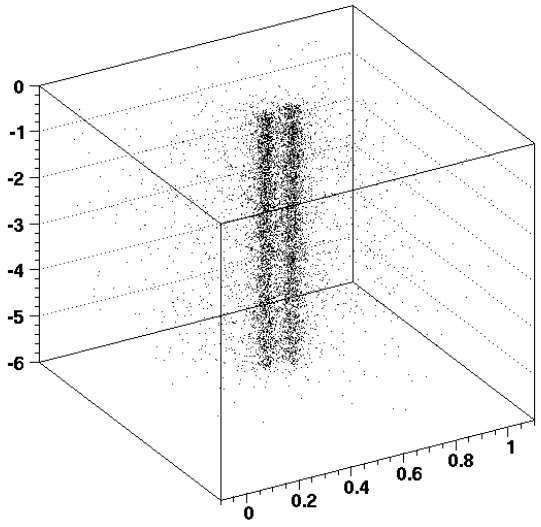

Figure 6: 3D plot of the conversion points of the photons inside the simulated HPPC.

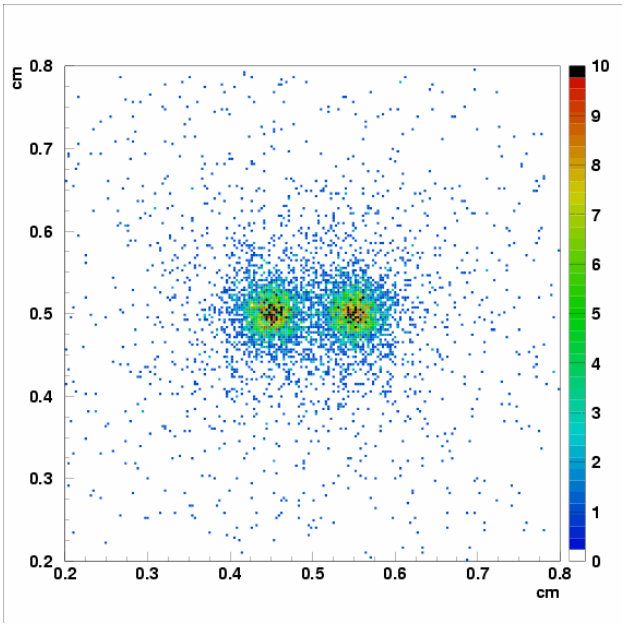

Figure 7: Bi-dimensional projection on the x-y plane of the conversion points of the photons.

detector producing an electron. A 2D projection is presented in Fig. 7. The sources are placed at 0.1 cm of distance from each-other, and have a gaussian profile with a sigma of 0.1 mm. As can be seen for most of the photons the smearing due to the interaction of the photons inside the detector is negligible, and the two sources may fairly be discriminated. There is a small fraction of photons scattered at long distance from the initial direction, resulting thus in a halo inside the detector. The fraction of this background can be estimated from the fit shown in Fig. 8 to be about 5%.

4.3. PET intrinsic limits

The intrinsic limit of the spatial resolution for a PET image come mainly from three contributions:

- the non-collinearity of the photons, due to a positron annihilation not at rest. This causes

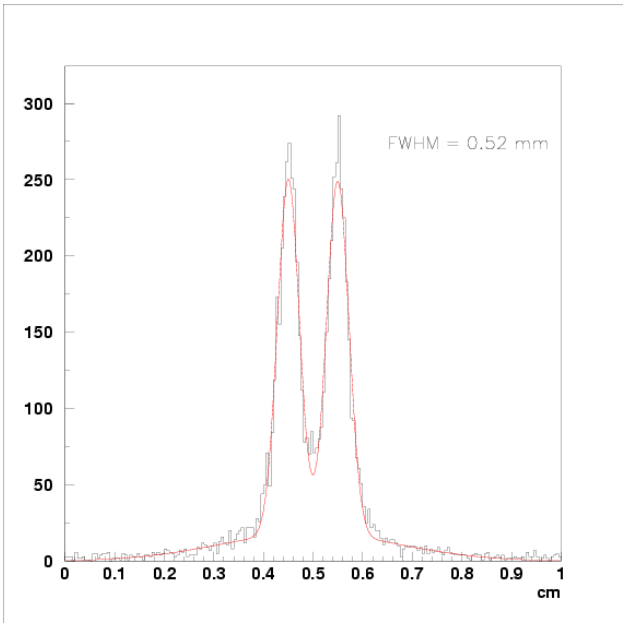

Figure 8: Gaussian fit of the profile of the photons scattered by the detector.

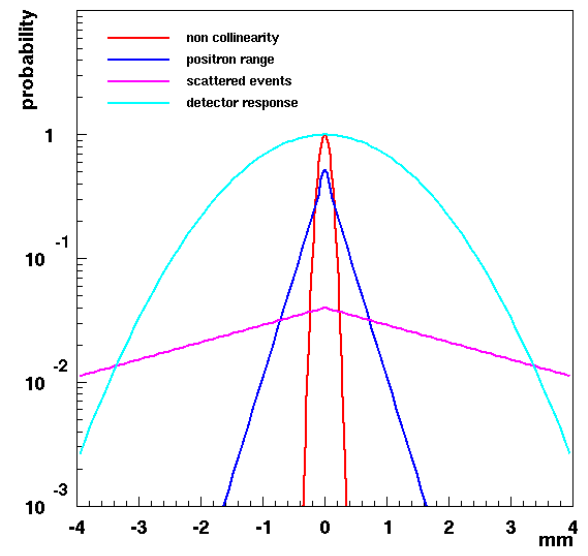

Figure 9: Principal contributions to the intrinsic spatial resolution of a PET with a ring diameter of 100 mm.

an error because in the reconstruction a 180° angle is assumed between the lines of flight. The contribution may be parametrized with a gaussian[5]

$$D(x) = exp(-\frac{x^2}{2\sigma^2})$$

where $\sigma \simeq 1$ mrad $\times d_s$, and d_s is the system diameter;

- the positron range inside the tissues, causing a photon production point different from the actual radio-tracer decay point. A double exponential properly describes this contribution [6][7]

  $D(x) = C_1 exp(-k_1 x) + (1 - C_1) exp(-k_2 x)$

  where

  $C_1 = 0.529;\ k_1 = 46.2 mm^{-1};\ k_2 = 3.75 mm^{-1}$

- a change in the direction of one or both photons due to Compton scattering inside the tissues. A simple parametrization is [8]

  $$D(x) = C_2 exp(-k_3 x)$$

  where

  $$C_2 = 0.04;\ k_3 = 0.32 mm^{-1}$$

Considering a possible diameter of 100 mm for a small animal PET scanner, and adding all the factors, a limit of about 0.5 mm FWHM is obtained. In Fig. 9 the detector response, as expected for the prototype described in section 2, is plotted as well. This is simply a gaussian having $\sigma_{res} = a/\sqrt{12}$, where $a = 4mm$ is the pitch of the readout for the first prototype. The intrinsic limit is still far to reach, thus suggesting that there is a lot of room for improvements in future prototypes.

5. Conclusions

A profitable R&D has been started on a new gaseous detector for medical imaging, in particular for PET applications. The proposed detector is a Hybrid Parallel Plate Chamber, exploiting the well known characteristics of RPCs, with an enhanced pointing to the detection of photons.

A time resolution of about 100 ps and a spatial resolution of 1 mm seem feasable. These performances are comparable with those of scintillators, although the efficiency for photons stays an order of magnitude lower with respect to crystals, a 1 mm resolution is obtained in the measurement of the Depth Of Interaction, allowing for a precise correction of the parallax error in the imaging reconstruction.

Taking into account the cheapness and the robustness of the detector, it can be considered a possible alternative in PET.

Acknowledgments

The authors wish to thank E.Iacuessa, S.Lauciani and G.Papalino for their technical help in preparing this work.

References

[1] See for example: Elhendy et al., J Nucl Med 43 (2002) 1634.
[2] See for example: M. A. Mandelkern, Ann. Rev. Nucl. Part. Sci. 45 (1995) 205.
[3] Nucl. Instr. Meth. 187 (1981) 377.
[4] "FLUKA: a multi-particle transport code", A. Fassò, A. Ferrari, J. Ranft, and P.R. Sala, CERN-2005-10 (2005), INFN/TC-05/11, SLAC-R-773
[5] J. Nucl. Med. 34 (1993) 101.
[6] Phys. Med. Biol. 44 (1999) 781.
[7] IEEE Trans. Nucl. Sci. 33 (1986) 565
[8] Proc. IEEE MIC 33 (2004) M2-177